The Effects of Atomic Scale Strain Relaxation on the Electronic Properties of Monolayer MoS_2

Daniel J. Trainer[1], Yuan Zhang[2], Fabrizio Bobba[1,3], Xiaoxing Xi[1], Saw-Wai Hla[2,4], Maria Iavarone[1]*

[1] Physics Department, Temple University, Philadelphia PA 19122, USA

[2] Center for Nanoscale Materials, Argonne National Laboratory, Lemont, IL 60439, USA

[3] Physics Department, University of Salerno, Fisciano (SA), 84084, Italy

[4] Physics & Astronomy Department, Ohio University, Athens, OH 45701, USA

The submitted manuscript has been created by UChicago Argonne, LLC, Operator of Argonne National Laboratory ("Argonne"). Argonne, a U.S. Department of Energy Office of Science laboratory, is operated under Contract No. DE-AC02-06CH11357. The U.S. Government retains for itself, and others acting on its behalf, a paid-up nonexclusive, irrevocable worldwide license in said article to reproduce, prepare derivative works, distribute copies to the public, and perform publicly and display publicly, by or on behalf of the Government.

ABSTRACT

The ability to control nanoscale electronic properties by introducing macroscopic strain is of critical importance for the implementation of 2D materials into flexible electronics and next generation strain engineering devices. In this work we correlate the atomic-scale lattice deformation with a systematic macroscopic bending of monolayer molybdenum disulfide films by using scanning tunneling microscopy and spectroscopy implemented with a custom-built sample holder to control the strain. Using this technique, we are able to induce strains of up to 3% before slipping effects take place and relaxation mechanisms prevail. We find a reduction of the quasiparticle bandgap of about 400 meV per percent local strain measured with a minimum gap of 1.2 eV. Furthermore, unintentional nanoscale strain relaxation of van der Waals monolayer sheets can negatively impact strain engineered device performance. Here we investigate such strain relaxation mechanisms that include 1D ripples and 2D wrinkles which alter the spatial electronic density of states and strain distribution on the atomic-scale.

KEYWORDS: molybdenum disulfide, monolayer, strain engineering, CVD, STM

Semiconducting transition metal dichalcogenides (TMDCs), such as molybdenum disulfide (MoS_2), possess enormous potential for next generation nanoelectronics as a result of their relatively large band gap and 2D nature. Like graphene,[1] single layer MoS_2 exhibits flexibility out of plane coupled with a high intrinsic tensile strength which allows the film to sustain up to 11% strain before rupturing.[2] It is theoretically predicted that tensile strain would strongly affect the bandgap of semiconducting TMDCs with the potential of closing the gap completely through the application of ~10% biaxial strain.[3–5] Furthermore, strain is expected to alter the charge carrier effective masses, dielectric properties,[6,7] thermal conductivity,[8,9] spin–orbit coupling[10–12] and electrical properties[13] and therefore, affect possible applications.[14,15] All of these properties make single layer MoS_2 a tantalizing candidate for components in future flexible devices such as mountable physiological monitoring devices, touch screens and flexible energy storage systems.[16–20] To date, a wide range of strategies have been exploited for applying strain to 2D TMDCs in nanomechanical devices, including the use of polymer sacrificial layers,[21] pre-patterned geometries,[22] and flexible[23–26] or piezoelectric substrates.[27] For nanoscale device applications, it is vital to understand the effect that macroscopic strain could have on the atomic-scale properties. Despite the myriad of existing literature, the nanoscale effect of a systematic strain and a direct measurement of strain relaxation effects are still elusive. Here, we investigate the effects of strain and strain relaxations on monolayer MoS_2 and provide atomic level details on their influence over the electronic properties.

RESULTS AND DISCUSSION

Single layer MoS_2 films are prepared by ambient pressure chemical vapor deposition (APCVD) on highly oriented pyrolytic graphite (HOPG). The details of the growth process can be found elsewhere (see Methods).[28] An atomic force microscopy (AFM) image of such a film is presented in Figure 1a, showing typical film morphologies consisting of triangular and hexagonal structures. Although, typically MoS_2 films grown on HOPG present islands of different numbers of layers, it is possible to identify the first layer of MoS_2 by STM as shown in Figure 1b. For our investigation, a tensile strain is applied to the film by bending the substrate using a custom-built sample holder (Figure 1c). When a slab is bent and there is no shear relaxation on either surface, the neutral plane of the slab will maintain the same length, but the top and bottom surface will experience a tensile and compressive strain, respectively. The nominal tensile strain on the surface of the slab can be defined by the following expression:

$$\varepsilon_{Nominal} = \frac{\tau}{2R} \tag{1}$$

where τ is the substrate thickness (in this case hundreds of microns) and R is the radius of curvature of the semi-circular wedge. The substrate then transfers the strain to the adhered MoS_2 film as schematically shown in Figure 1d. The STM scanner was aligned such that the fast scan direction, or the X-direction, is perpendicular to the bending axis and therefore, the slow scan direction, or the Y-direction, is parallel to the bending axis.

Atomic resolution STM topographies of MoS_2 monolayer films with nominal strain of 0% and 4.9% are reported in Figures 2a and 2b, respectively. To quantify the local strain, we analyze these images by using a procedure similar to the Lawler-Fujita[29] drift correction (see Supplementary Section I). This algorithm calculates the displacement between each atomic position in the measured lattice and their expected position in an ideal, unstrained lattice. The

collection of displacement values over each atom in the lattice generates the displacement field u(r) which can be deconstructed into the x- and y-direction components, namely $u_x(x)$ and $u_y(y)$. These values are plotted as a function of distance in Figures 2c and 2d for nominal strain of 0% and 4.9%, respectively. The strain tensor can be directly calculated by taking the derivative of u(r) along the lattice vectors. Therefore, we define the average x-direction (y-direction) strain of each STM measurement as the slope of the linear fit to the $u_x(x)$ vs. x ($u_y(y)$ vs. y) data.In the case of the 0% nominal strain film shown in Figure 2a and 2c, the measured strain values for the x- and y-direction are -0.12% and 0.21%. These values change to 2.67% and -1.16% for the sample shown in Figure 2b and 2d with the maximum nominal strain of 4.9% (*i.e.* bent to a 1mm radius of curvature). The small strains measured in the samples with 0% nominal strain can come from the surface preparation prior to the STM measurement. The films are heated to 300ºC to clean the surface in UHV before being cooled to 4K on the STM scanner. The thermal expansion of these processes can explain the small strain observed in the film with 0% nominal strain.

MoS_2 has a positive Poisson's ratio[30,31] which means that the crystal will respond to a tensile stretching in one direction by compressing in the perpendicular direction. Therefore, we expect the tensile strain imposed on the film to be in the x-direction of our scanner and the corresponding compressive strain to be in the y-direction. Figure 2e presents the average measured strain in both directions plotted as a function of nominal strain for all samples measured. Here, the measured x-direction strain increases almost linearly until 2.5% nominal strain where the maximum local measured strain is always less than the expected nominal value. At this value of nominal strain of 2.5% we find that there are areas of the sample where there is little to no average measured strain, corresponding to a relaxed lattice. This is true to a larger

extent for higher values of the nominal strain, where in the case of 4.9% the maximum local strain measured is only 3.1%. The strain in the y-direction shows a similar trend in the compressive direction. This behavior of the local strain as a function of the nominal strain reveals that the film is slipping with respect to the substrate, likely due to van der Waals nature of the two materials and, therefore to a weak adhesion at the interface.[32,33]

The Poisson ratio is defined as $\nu = - \varepsilon_y/\varepsilon_x$ only if the stress in the y-direction is fully relaxed after the material is strained in the x-direction. Assuming this form, we calculate a Poisson ratio of 0.44 from our measurements. This number indeed deviates from the theoretical value of ~0.2 for MoS_2.[34] Considering the method which we are straining the MoS_2 films and their unavoidable interaction with the substrate, however, we do not expect the normal direction to be allowed to relax freely. Specifically, we rely on the substrate to transfer the tensile strain to the film in the x direction, but it will also transfer a compressive strain in the y direction since HOPG has a positive Poison's ratio as well. Therefore, we do not expect our films to exhibit the theoretical Poisson's ratio of ~0.2 because the unavoidable interaction with the substrate will inhibit the normal direction stress relaxation.

To correlate the quasiparticle density of states with the local strain, tunneling spectra were acquired at different atomic sites within the imaged area from which the local strain was obtained. These spectra were then averaged, and their quasiparticle band gap was extracted by finding the intersection point between a linear fit close to the band edge and zero conductance. Figure 3a shows representative spectra obtained at different values of nominal strain. Since, as described earlier, different areas of a sample with a given nominal strain can have varying local strain, the representative curves have been chosen to correspond to values of local strain closest to the nominal strain. Figure 3b presents a summary of the quasiparticle band gap extracted

from the tunneling spectra plotted as a function of nominal strain. Here, the quasiparticle band gap decreases at one rate up until a nominal strain of 2.5% and at a much slower rate from 2.5% to 4.9%. Furthermore, at the nominal strain of 5% there are areas of the sample where the quasiparticle band gap resembles that of a relaxed film. These observations are consistent with film slipping or other strain relaxation mechanisms taking place. In Figure 3c the quasiparticle band gap is plotted as a function of the local measured strain. Our measurements reveal a clear trend for the positive tensile strain, where the quasiparticle band gap reduces at a rate of approximately 400meV/% tensile strain. The effect of strain on the optical band gap of single layer MoS_2 and related materials has been well documented.[24,27,35–37] Photoluminescence measurements have confirmed theoretical predictions that strain could cause a bandgap reduction of ~70 meV/% strain for the direct gap transition, and ~110 meV/% strain for the indirect gap transition in bilayer MoS_2.[3,23] However, the beam diameter of such experiments is at best a few hundred nanometers[35,36] limiting their capacity to study the effect of strain on the atomic scale. In addition, the quasiparticle bandgap, which differs from the optical gap by the value of the exciton binding energy,[37] has not been studied as a function of systematic strain. Although our measured bandgap reduction rate is higher than those reported from the optical bandgap in literature[33] it is much closer to a recent STM study measuring strain in TMDCs. In that study, Zhang *et al.*[34] measured a bandgap reduction rate of 500 meV/% strain in lateral heterostructures comprised of WSe_2-MoS_2 by scanning tunneling spectroscopy. Note that the optical band gap is dominated by the direct gap whereas the quasiparticle bandgap, as measured by scanning tunneling spectroscopy, is an integrated average over k-space. It should also be noted that all the spectra reported here were acquired away from edges, grain boundaries and defects which are known to alter the local density of states. In addition, the bandgap has been found to be affected

by relative orientation of the MoS_2 monolayer with respect to the HOPG substrate. However this effect has been measured on this system in earlier measurements to be less than 150meV.[39] Therefore, we expect the changes in bandgap to be predominantly due to strain.

The weak inter-layer coupling between the MoS_2 and HOPG makes slipping a plausible strain relaxation mechanism. Figure 4a presents two parallel ripples induced by such slipping of a MoS_2 monolayer with a nominal strain of 3.3%. Figure 4b shows a magnified atomic scale STM image of the right most ripple. Intuitively, ripples in such MoS_2 sheets are expected to be caused by a compressive strain. Formation of such ripples have been predicted for a compressive strain greater than 2%by molecular dynamics simulations .[32] Here we investigate how these ripples influence the local electronic properties by acquiring tunneling spectra (Figure 4c) along the dotted line in Figure 4b. The measurements show an abrupt increased in energy gap by expanding the valence band maximum (VBM) for ~ 150 meV on top of the ripple and it maintains for the region outside of the ripple. . Figure 4d presents a dI/dV map (conductance map) acquired at a fixed energy just below the VBM at -1.72 eV. The conductance map reveals that the increase of states at the VBM (higher intensities) is localized between the parallel ripples, with the ripples forming the boundaries. This structure presents possibilities for strain engineering of conduction channels in MoS_2, and similar materials.

Next, the modified Lawler-Fujita algorithm has been used to calculate the strain field at each atomic position in the direction perpendicular to the ripples. To highlight variations in the strain field, the average slope of the displacement field has been subtracted to give relative values of strain. The average strain removed in the direction perpendicular to the ripples was naturally compressive and approximately 7.6% (Supplemental Note II), and the corresponding

strain-field map is displayed in Figure 4e overlaid on the topography shown in Figure 4b. It is expected that the region between the two ripples should yield a higher relative tensile strain than that away from the two ripples. It is also intuitive that the region on either side of the ripple would experience a compressive strain relative to the surrounding regions. While both expectations are observed, surprisingly there are unexpected oscillations in strain moving away from the two ripples that are not apparent in the topography. This indicates that the strain responsible for the formation of the ripple is not localized on top of the ripple but manifests itself as oscillations which extend at least 15nm away from the ripple.

To compare the local strain field with the local electronic properties, the relative strain (obtained after subtraction of the average strain) in the direction perpendicular to the ripple in Figure 4e is plotted in Figure 4f together with the bandgap extracted from Figure 4c. Here, the 150meV shift of the bandgap occurs directly at the ripple location where there is the highest relative compression. In addition, we find that the average strain also affects the bandgap away from the ripple as it is reduced compared to that of the relaxed MoS_2 layer. The changes in the band gap in the presence of large compressive strains appear to be significantly lower than those found in the presence of tensile strain (Figure 3c). This finding is in accord with the prediction based on DFT calculations[40] where the compressive strain is expected to have a smaller effect on the quasiparticle band gap compared with the tensile strain.

Additional relaxation mechanisms are found when the film is subjected to a nominal strain of 4.9%. Here, several regions exhibit inhomogeneous moiré pattern that is typically observed close to defects, indicating that the film undergoes a partial delamination and is well adhered to the substrate only in the regions that display the moiré pattern. An example is displayed in Figure 5a where the film is bunched around a defect with a small area showing a

moiré pattern. The strain map corresponding to Figure 5a is displayed in Figure 5b, which reveals an inhomogeneous strain-field that undergoes an abrupt transition from tensile to compressive strain on the defect and along the border of the moiré region. Here, the area showing the moiré pattern exhibits a compressive strain compared to the surrounding area. To elucidate the electronic properties of such a defect, two line profiles of point spectra were taken perpendicular to each other. The two sequences of spectra are shown in the lower panels of Figure 5c and 5d, while the paths, along which the spectra were acquired, are shown in the top panels of Figure 5c and 5d, respectively. The profile taken over the central defect reveal localized in-gap states that appear directly at the defect site. The profile in Figure 5d shows that the magnitude of the gap increases by the VBM shifting outward in the region over the moiré pattern. To focus on the spatial variation in the electronic density of states, conductance maps were taken at a variety of different energies close to the conduction band maximum (CBM) and the VBM shown in Figures 5e-j and Figures 5k-p, respectively. An increase of conductance is observed at the defect site at an energy close to 1eV while a suppression of conductance is observed at around 0.7eV. Close to the VBM there are localized in-gap states at -1eV and -1.7eV that are revealed in a radius of about ½ nm surrounding the defect site. The spatial variation of the VBM displays a region of higher band gap corresponding to the less tensile strained region of the moiré pattern in topography. This appears as a low conductance region in the conductance map at energies close to the VBM around -2 eV. In this region the point spectra show an outward shift of the VBM (bottom panel of Figure 5d). While the variation at the CBM is localized over the central defect, the variation of the VBM has a clear correlation with the shape of the moiré pattern in topography, where the conductance at the VBM shows a strong increase along the edge of the moiré pattern. The variation of the quasiparticle band gap, which

spatially follows the edges of the delamination of the film, is likely due to a combination of the varying local strain-field as well as the changing Coulomb screening due to the delamination of the film from the substrate.

CONCLUSIONS

We have successfully applied strains of up to about 3% on monolayer MoS_2 films using a custom-built sample holder and correlated the macroscopic nominal strain with the local atomic-scale strain. Furthermore, we have correlated the local strain and the quasiparticle band gap which shows a reduction of about 400meV per percent local strain. Within the same sample, with a nominal strain of 2.5% or higher, there are regions that show local strain consistently lower than the nominal applied strain, likely due to the weak van der Waals nature of the MoS_2 film and substrate. In these regions the film experiences strain relaxation that inhibits the application of strain greater than 3% using this method. Relaxation mechanisms that have been observed include formation of one-dimensional ripples and two-dimensional wrinkles that alter the local electronic density of states. Tunneling spectroscopy shows a reduction of the band gap at the ripple location with perturbation of the local density of states that extends to a distance of at least 15 nm away from the ripple. Two-dimensional wrinkles found on samples with higher nominal strain, are characterized by areas displaying inhomogeneous moiré patterns surrounding or near various defects. This suggest that the film has a nonuniform adhesion with the substrate, which allows for the partial delaminating and slipping of the film with respect to the substrate. This causes formation of two-dimensional wrinkles that alter the local electronic properties of the film. These processes illustrate the weak coupling between the van der Waals layers

displayed between film and substrate. Despite this weak interaction we show that it is possible to impose strain of up to 3% using heterostructures of this kind.

It is also important to note that compressive strain areas have a smaller effect on the quasiparticle band gap. Lu, *et al*.[40] used DFT to investigate positive and negative strain on monolayer MoS_2 finding that not only is the band gap smaller for positive strain than it is for its negative counterpart, but that the band gap initially increases with negative strain before reducing again. This is explained to be primarily a result of the change in length of the Mo-S bond which is naturally smaller for compressive strains than for the tensile strains. In the same study they also find that there is not a significant difference between uniaxial and isotropic strains in terms of their effect on the band gap of monolayer MoS_2. This indicates that for our study, the relative orientation between the crystallographic axis and the bending axis has little influence on how the strain effects the quasiparticle band gap.

METHODS

Film Growth. Single layer MoS_2 films were grown on highly pyrolytic graphite (HOPG) substrates using the ambient pressure chemical vapor deposition technique described previously[28]. The precursors used in the deposition were ~12mg of MoO_3 (≥99.5% Sigma Aldrich) and ~100mg of S powder (≥99.5% Sigma Aldrich). Otherwise the set up and heating steps were identical to those previously described[28]. The MoS_2 films are deposited on HOPG to allow STM measurements while at the same time preventing changes of

the electronic properties of MoS_2 due to the interaction with the substrate and/or avoid any possible damage of the film associated with transfer techniques.

Method used to apply strain. The sample holder is comprised of two Cu pieces which are supported by an Omicron sample plate. The bottom piece is a semi-circular wedge which fits under the top Cu block which has a space removed with the exact dimensions of the wedge. There is a hole on the top of the block through which the STM tip can access the sample. Alignment of the tip at the top of the curvature is performed optically. The sample is placed between these two pieces and as the block is gently screwed to the sample plate it bends the sample, making it adhere to the radius of curvature of the semi-circular wedge.

STM/STS. Scanning tunneling microscopy and spectroscopy measurements were carried out using a Unisoku STM with PtIr tip at Temple University for the measurement in Figure 1b and a Createc STM with a W tip at the Center for Nanoscale Materials for the rest of the measurements. Both sets of measurements were carried out in an ultra-high vacuum ($< 10^{-10}$ Torr) at T = 4.2 K. All STM tips used in this experiment were previously prepared on Au or Ag single crystals. The STM images were recorded in constant current mode with set point parameters listed in the Figures captions. The individual dI/dV spectra found in Figure 3 were recorded by taking the numerical derivative of the measured I-V curves and applying a 10-point Savitzky-Golay smoothing. The maps and line spectroscopy in Figures 4 and 5 were obtained using a lock-in technique with a modulation voltage of 30mV and a modulation frequency of 3.1kHz.

AFM. Atomic force microscopy images were acquired in tapping mode using a Veeco Dimension Icon SPM with an Antimony (n) doped Si tip having a nominal tip radius of 10 nm (Veeco, NCHV). In this mode, the cantilever is driven to oscillate at its resonance frequency of 320 Hz by applying an AC voltage to the z-piezo. As long as the tip is far away from the sample, no interaction is recorded and the oscillation amplitude remains constant. Once the cantilever is moved closer to the sample, the tip starts touching the surface intermittently. As a consequence, changes in the cantilever oscillation amplitude are induced by the Van der Waals interaction. In such a scenario, the amplitude modulations recorded while scanning on the surface are caused by the sample roughness. Here, a feedback loop is used to fix the tip-sample separation point-by-point in order to keep the amplitude constant. The adjustments in tip-sample distance, driven by the feedback loop, are thus a measure of sample topography. AFM measurements were carried out under ambient conditions.

REFERENCES

(1) Lee, C.; Wei, X.; Kysar, J. W.; Hone, J. Measurements of the Elastic Properties and Intrinsic Strength of Monolayer Graphene. *Science* **2008**, *321*, 385.

(2) Bertolazzi, S.; Brivio, J.; Kis, A. Stretching and Breaking of Ultrathin MoS2. *ACS Nano* **2011**, *5*, 9703–9709.

(3) Johari, P.; Shenoy, V. B. Tuning the Electronic Properties of Semiconducting Transition Metal Dichalcogenides by Applying Mechanical Strains. *ACS Nano* **2012**, *6*, 5449–5456.

(4) Yue, Q.; Kang, J.; Shao, Z.; Zhang, X.; Chang, S.; Wang, G.; Qin, S.; Li, J. Mechanical and Electronic Properties of Monolayer MoS2 under Elastic Strain. *Phys. Lett. A* **2012**, *376*, 1166–1170.

(5) Shi, H.; Pan, H.; Zhang, Y.-W.; Yakobson, B. I. Quasiparticle Band Structures and Optical Properties of Strained Monolayer MoS2 and WS2. *Phys. Rev. B* **2013**, *87*, 155304.

(6) Dong, L.; Namburu, R. R.; O'Regan, T. P.; Dubey, M.; Dongare, A. M. Theoretical Study on Strain-Induced Variations in Electronic Properties of Monolayer MoS2. *J. Mater. Sci.* **2014**, *49*, 6762–6771.

(7) Wang, L.; Kutana, A.; Yakobson, B. I. Many-Body and Spin-Orbit Effects on Direct-Indirect Band Gap Transition of Strained Monolayer MoS2 and WS2. *Ann. Phys. (Berlin, Ger.)* **2014**, *526*, L7–L12.

(8) Kumar, A.; Ahluwalia, P. K. Mechanical Strain Dependent Electronic and Dielectric Properties of Two-Dimensional Honeycomb Structures of MoX2 (X=S, Se, Te). *Phys. B (Amsterdam, Neth.)* **2013**, *419*, 66–75.

(9) Bhattacharyya, S.; Pandey, T.; Singh, A. K. Effect of Strain on Electronic and Thermoelectric Properties of Few Layers to Bulk MoS2. *Nanotechnology* **2014**, *25*, 465701.

(10) Rostami, H.; Roldán, R.; Cappelluti, E.; Asgari, R.; Guinea, F. Theory of Strain in Single-Layer Transition Metal Dichalcogenides. *Phys. Rev. B* **2015**, *92*, 195402.

(11) Cheiwchanchamnangij, T.; Lambrecht, W. R. L.; Song, Y.; Dery, H. Strain Effects on the Spin-Orbit-Induced Band Structure Splittings in Monolayer MoS2 and Graphene. *Phys. Rev. B* **2013**, *88*, 155404.

(12) Koskinen, P.; Fampiou, I.; Ramasubramaniam, A. Density-Functional Tight-Binding Simulations of Curvature-Controlled Layer Decoupling and Band-Gap Tuning in Bilayer MoS2. *Phys. Rev. Lett.* **2014**, *112*, 186802.

(13) Harada, N.; Sato, S.; Yokoyama, N. Computational Study on Electrical Properties of Transition Metal Dichalcogenide Field-Effect Transistors with Strained Channel. *J. Appl. Phys.* **2014**, *115*, 034505.

(14) Sengupta, A.; Ghosh, R. K.; Mahapatra, S. Performance Analysis of Strained Monolayer MoS2 MOSFET. *IEEE Trans. Electron Devices* **2013**, *60*, 2782–2787.

(15) Mohammad Tabatabaei, S.; Noei, M.; Khaliji, K.; Pourfath, M.; Fathipour, M. A First-Principles Study on the Effect of Biaxial Strain on the Ultimate Performance of Monolayer MoS2 -Based Double Gate Field Effect Transistor. *J. Appl. Phys.* **2013**, *113*, 163708.

(16) Feng, J.; Qian, X.; Huang, C.-W.; Li, J. Strain-Engineered Artificial Atom as a Broad-Spectrum Solar Energy Funnel. *Nat. Photonics* **2012**, *6*, 866–872.

(17) Kim, S. J.; Choi, K.; Lee, B.; Kim, Y.; Hong, B. H. Materials for Flexible, Stretchable Electronics: Graphene and 2D Materials. *Annu. Rev. Mater. Res.* **2015**, *45*, 63–84.

(18) Yoon, J.; Park, W.; Bae, G.-Y.; Kim, Y.; Jang, H. S.; Hyun, Y.; Lim, S. K.; Kahng, Y. H.; Hong, W.-K.; Lee, B. H.; Ko, H. C. Highly Flexible and Transparent Multilayer MoS2 Transistors with Graphene Electrodes. *Small* **2013**, *9*, 3295–3300.

(19) Xu, H.; Wu, J.; Feng, Q.; Mao, N.; Wang, C.; Zhang, J. High Responsivity and Gate Tunable Graphene-MoS2 Hybrid Phototransistor. *Small* **2014**, *10*, 2300–2306.

(20) Akinwande, D.; Petrone, N.; Hone, J. Two-Dimensional Flexible Nanoelectronics. *Nat. Commun.* **2014**, *5*, 5678.

(21) Zhu, H.; Wang, Y.; Xiao, J.; Liu, M.; Xiong, S.; Wong, Z. J.; Ye, Z.; Ye, Y.; Yin, X.; Zhang, X. Observation of Piezoelectricity in Free-Standing Monolayer MoS2. *Nat. Nanotechnol.* **2015**, *10*, 151–155.

(22) Lloyd, D.; Liu, X.; Christopher, J. W.; Cantley, L.; Wadehra, A.; Kim, B. L.; Goldberg, B. B.; Swan, A. K.; Bunch, J. S. Band Gap Engineering with Ultralarge Biaxial Strains in Suspended Monolayer MoS2. *Nano Lett.* **2016**, *16*, 5836–5841.

(23) He, K.; Poole, C.; Mak, K. F.; Shan, J. Experimental Demonstration of Continuous Electronic Structure Tuning via Strain in Atomically Thin MoS2. *Nano Lett.* **2013**, *13*, 2931–2936.

(24) Zhu, C. R.; Wang, G.; Liu, B. L.; Marie, X.; Qiao, X. F.; Zhang, X.; Wu, X. X.; Fan, H.; Tan, P. H.; Amand, T.; Urbaszek, B. Strain Tuning of Optical Emission Energy and Polarization in Monolayer and Bilayer MoS2. *Phys. Rev. B* **2013**, *88*, 121301.

(25) Conley, H. J.; Wang, B.; Ziegler, J. I.; Haglund, R. F.; Pantelides, S. T.; Bolotin, K. I. Bandgap Engineering of Strained Monolayer and Bilayer MoS2. *Nano Lett.* **2013**, *13*, 3626–3630.

(26) Desai, S. B.; Seol, G.; Kang, J. S.; Fang, H.; Battaglia, C.; Kapadia, R.; Ager, J. W.; Guo, J.; Javey, A. Strain-Induced Indirect to Direct Bandgap Transition in Multilayer WSe2. *Nano Lett.* **2014**, *14*, 4592–4597.

(27) Hui, Y. Y.; Liu, X.; Jie, W.; Chan, N. Y.; Hao, J.; Hsu, Y.-T.; Li, L.-J.; Guo, W.; Lau, S. P. Exceptional Tunability of Band Energy in a Compressively Strained Trilayer MoS2 Sheet. *ACS Nano* **2013**, *7*, 7126–7131.

(28) Trainer, D. J.; Putilov, A. V.; Di Giorgio, C.; Saari, T.; Wang, B.; Wolak, M.; Chandrasena, R. U.; Lane, C.; Chang, T.-R.; Jeng, H.-T.; Lin, H.; Kronast, F.; Gray, A. X.; Xi, X.X.; Nieminen, J.; Bansil, A.; Iavarone, M. Inter-Layer Coupling Induced Valence Band Edge Shift in Mono- to Few-Layer MoS2. *Sci. Rep.* **2017**, *7*, 40559.

(29) Lawler, M. J.; Fujita, K.; Lee, J.; Schmidt, A. R.; Kohsaka, Y.; Kim, C. K.; Eisaki, H.; Uchida, S.; Davis, J. C.; Sethna, J. P.; Kim, E.-A. Intra-Unit-Cell Electronic Nematicity of the High-Tc Copper-Oxide Pseudogap States. *Nature* **2010**, *466*, 347–351.

(30) Woo, S.; Park, H. C.; Son, Y.-W. Poisson's Ratio in Layered Two-Dimensional Crystals. *Phys. Rev. B* **2016**, *93*, 075420.

(31) Woo, S.; Park, H. C.; Son, Y.-W. Erratum: Poisson's Ratio in Layered Two-Dimensional Crystals [Phys. Rev. B **93**, 075420 (2016)]. *Phys. Rev. B* **2016**, *94*, 239901.

(32) Wang, J.; Namburu, R. R.; Dubey, M.; Dongare, A. M. Origins of Ripples in CVD-Grown Few-Layered MoS2 Structures under Applied Strain at Atomic Scales. *Sci. Rep.* **2017**, *7*, 40862.

(33) Roldan, R.; Castellanos-Gomez, A.; Cappelluti, E.; Guinea, F. Strain Engineering in Semiconducting Two-Dimensional Crystals. *J. Phys.: Condens. Matter* **2015**, *27*, 313201.

(34) Zhang, C.; Li, M.-Y.; Tersoff, J.; Han, Y.; Su, Y.; Li, L.-J.; Muller, D. A.; Shih, C.-K. Strain Distributions and Their Influence on Electronic Structures of WSe2–MoS2 Laterally Strained Heterojunctions. *Nat. Nanotechnol.* **2018**, *13*, 152–158.

(35) Li, H.; Contryman, A. W.; Qian, X.; Ardakani, S. M.; Gong, Y.; Wang, X.; Weisse, J. M.; Lee, C. H.; Zhao, J.; Ajayan, P. M.; Li, J.; Manoharan, H. C.; Zheng, X. Optoelectronic Crystal of Artificial Atoms in Strain-Textured Molybdenum Disulphide. *Nat. Commun.* **2015**, *6*, 7381.

(36) Liu, Z.; Amani, M.; Najmaei, S.; Xu, Q.; Zou, X.; Zhou, W.; Yu, T.; Qiu, C.; Birdwell, A. G.; Crowne, F. J.; Vajtai, R.; Yakobson, B. I.; Xia, Z.; Dubey M.; Ajayan, P. M.; Lou, J. Strain and Structure Heterogeneity in MoS2 Atomic Layers Grown by Chemical Vapour Deposition. *Nat. Commun.* **2014**, *5*, 5246.

(37) Rice, C.; Young, R. J.; Zan, R.; Bangert, U.; Wolverson, D.; Georgiou, T.; Jalil, R.; Novoselov, K. S. Raman-Scattering Measurements and First-Principles Calculations of Strain-Induced Phonon Shifts in Monolayer MoS2. *Phys. Rev. B* **2013**, *87*, 081307(R).

(38) Ugeda, M. M.; Bradley, A. J.; Shi, S.-F.; da Jornada, F. H.; Zhang, Y.; Qiu, D. Y.; Ruan, W.; Mo, S.-K.; Hussain, Z.; Shen, Z.-X.; Wang, F.; Louie, S. G.; Crommie, M. F. Giant Bandgap

Renormalization and Excitonic Effects in a Monolayer Transition Metal Dichalcogenide Semiconductor. *Nat. Mater.* **2014**, *13*, 1091–1095.

(39) Trainer, D. J.; Putilov, A. V.; Wang, B.; Lane, C.; Saari, T.; Chang, T.-R.; Jeng, H.-T.; Lin, H.; Xi, X.; Nieminen, J.; Bansil, A.; Iavarone, M. Moiré Superlattices and 2D Electronic Properties of Graphite/MoS2 Heterostructures. *J. Phys. Chem. Solids* **2019**, 128, 325-330.

(40) Lu, P.; Wu, X.; Guo, W.; Zeng, X. C. Strain-Dependent Electronic and Magnetic Properties of MoS2 Monolayer, Bilayer, Nanoribbons and Nanotubes. *Phys. Chem. Chem. Phys.* **2012**, *14*, 13035.

ASSOCIATED CONTENT

Conflict of Interest: The authors declare no competing financial interests.Supporting Information Available

Additional Information on the strain estimation and modified real space Lawler-Fujita Algorithm. This material is available free of charge *via* the Internet at http://pubs.acs.org.

AUTHOR INFORMATION

Corresponding Author

*E-mail iavarone@temple.edu

Author Contributions. D. J. Trainer, F. Bobba and Yuan Zhang performed low temperature STM/STS measurements at the Center for Nanoscale Materials at Argonne National Laboratory under guidance of M. Iavarone and Saw Hla. D. J. Trainer fabricated MoS_2 films under guidance

of X. X. Xi and he characterized the samples with AFM/STM. The manuscript was written through contributions of all authors. All authors have given approval to the final version of the manuscript.

ACKNOWLEDGEMENTS

This work was supported primarily the Center for Complex Materials from First Principles (CCM), an Energy Frontier Research Center funded by the U.S. Department of Energy, Office of Science, Basic Energy Sciences under Award #SC0012575 (STM measurements, AFM measurements and thin films growth). Use of the Center for Nanoscale Materials, an Office of Science user facility, was supported by the US Department of Energy, Office of Science, Office of Basic Energy Sciences, under contract no. DE-AC02-06CH11357.

Figures

Figure 1. Strain imposing device. a, Large scale AFM topography portraying a typical morphology of the as grown CVD MoS_2 film on the graphite substrate. Scale bar represents 500nm. **b,** STM topography showing the step edge between the single layer of MoS_2 and the underlying HOPG substrate (V_t = -2.5 V, I_t = 10 pA). Scale bar represents 50nm. **c,** The custom built sample holder used to control the nominal strain on the sample. **d,** A cartoon depiction of a substrate transmitting strain to a film by bending.

Figure 2. Atomic scale strain. a,b Atomic resolution STM iamges of single layer MoS_2 film with nominal strain of 0% (V = -1.0 V, I = 110 pA) and 4.9% **,** respectively (V_t = -1.5 V, I_t = 55 pA). Scale bars represent 2nm. **c,d** Real space determination of lattice deformation of Figure 2a **(c)** and Figure 2b **(d)**. The black squares and red circles represent the lattice distortion in the x-direction and y-direction as a function of distance in x and y, respectively. **e,** Lattice strain in the x-direction (perpendicular to the bending axis) measured as a function of nominal strain. The inset shows corresponding strain measured in the y-direction (parallel to the bending axis). The error bars represent a 95% confidence interval for the distribution of displacement field values.

Figure 3. Effect of atomic scale strain on the quasiparticle bandgap. a, A series of vertically offset tunneling spectra taken on monolayer MoS_2 films displaying the minimum gap on each respective radii of curvature (V_t = +1.5 V or +1.0 V, I_t = 100 pA). **b,** A summary of the evolution of the quasiparticle band gap (E_g) as a function of the nominal strain. **c,** Corresponding summary of the evolution of the quasiparticle band gap as a function of the measured strain along the x-direction. The blue shaded region represents a compressive strain whereas the red shaded region represents a tensle strain. The dashed red line represents a linear-fit of the data displaying a tensile strain. The gap has been determined by making a linear fit to the conductance spectrum within a voltage window at the valence band and conduction band edges and finding the zero intercept. All error bars represent +/- 95% confidence interval to the mean.

Figure 4. Electronic structure of a rippled monolayer. a, resolution 3-D STM image showing two parallel ripples on monolayer MoS_2 (V_t = +0.8 V, I_t = 100 pA). **b,** An enhanced view of the area marked with a rectangle in (a). (V_t = +0.8 V, I_t = 100 pA). **c,** Tunneling spectra acquired along the dotted arrow in Figure 4b (V_t = +1.0 V, I_t = 110 pA). **d,** A dI/dV map corresponding to

(b) acquired at -1.72 eV. The vertical line in (c) indicates the energy at which the dI/dV mp istaken **e,** A map of the spatial variation of the relative strain-field in the direction perpendicular to the ripples overlaid on the 3D topography shown in Figure 4b. The average strain (slope of u_x vs. x) was removed to emphasize the variation in strain. **f,** The averaged relative strain across the height of Figure 4c from left to right plotted along with the quasiparticle band gap extracted from Figure 4c. All scale bars represent 5nm.

Figure 5. Spatial variation of the density of states over an inhomogeneous moiré pattern on a monolayer. a, resolution 3-D STM image showing the inhomogeneous moiré pattern at a defect site (V_t = -1.0V, I_t = 110pA). **b,** A map of the spatial variation of the absolute x-direction strain field overlaid on the 3D topography from the area outlined by the dashed box in Figure 5a. All scale bars represent 2nm. **c,d** Tunneling spectra maps taken along the lines shown in their respective STM images (insets). **e – p,** A sequence of dI/dV maps showing the evolution of the local density of states at energies near the conduction band **(e – j)** and the valence band edges **(k – p)** (V_t = +1.0V, I_t = 110pA).

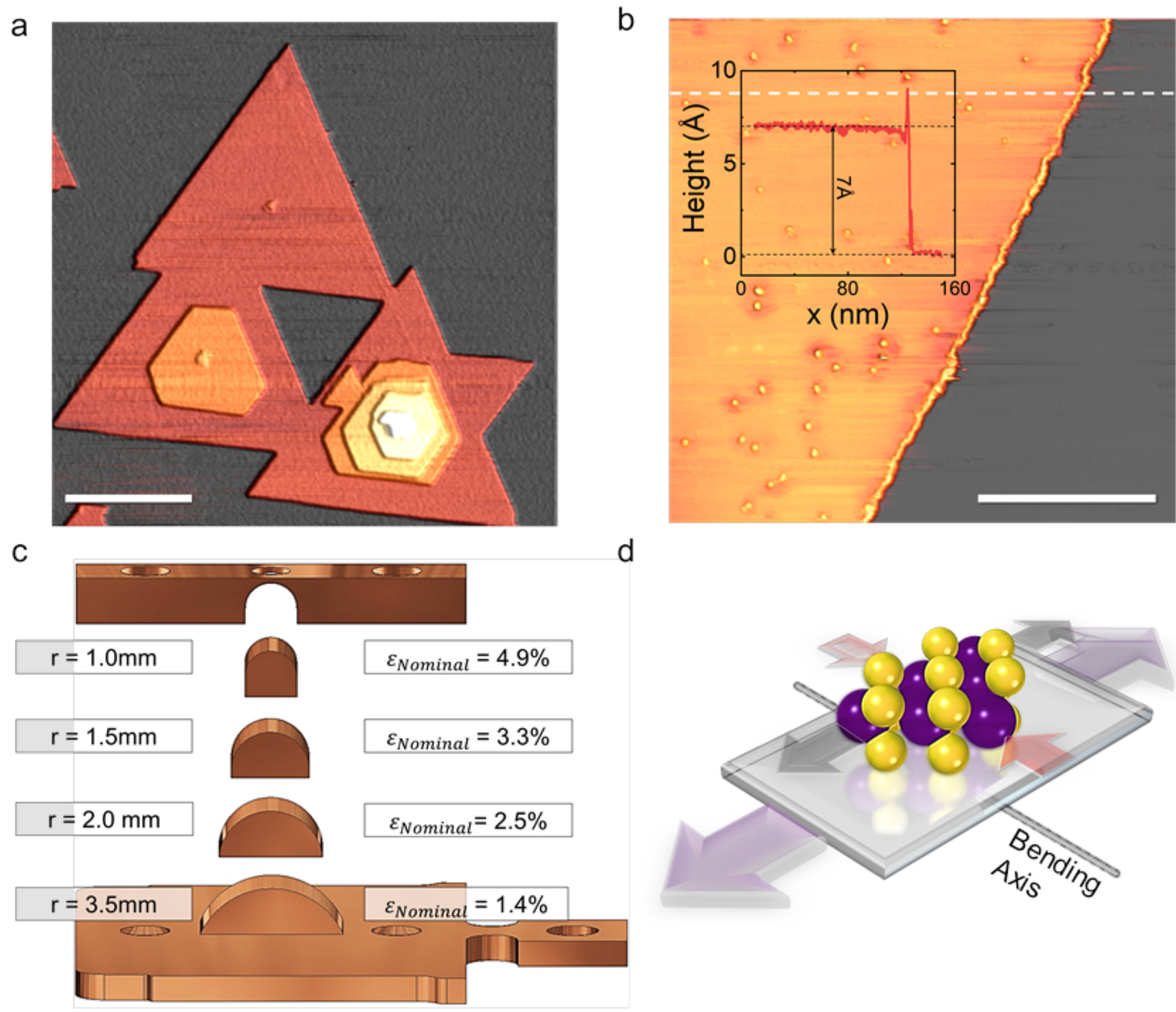

FIG.1

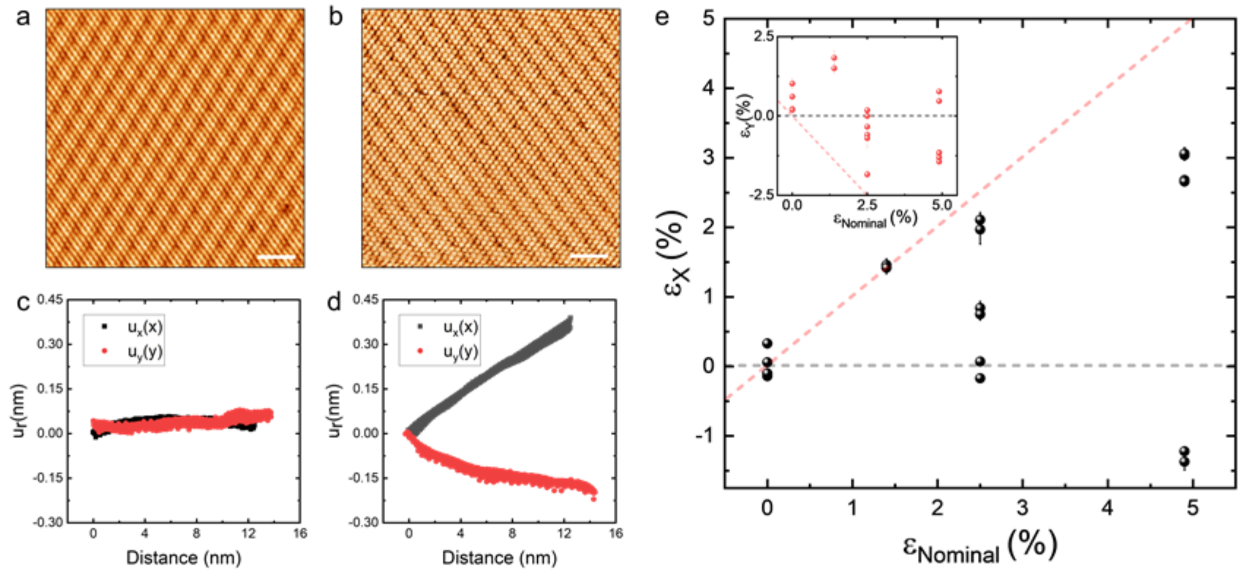

FIG.2

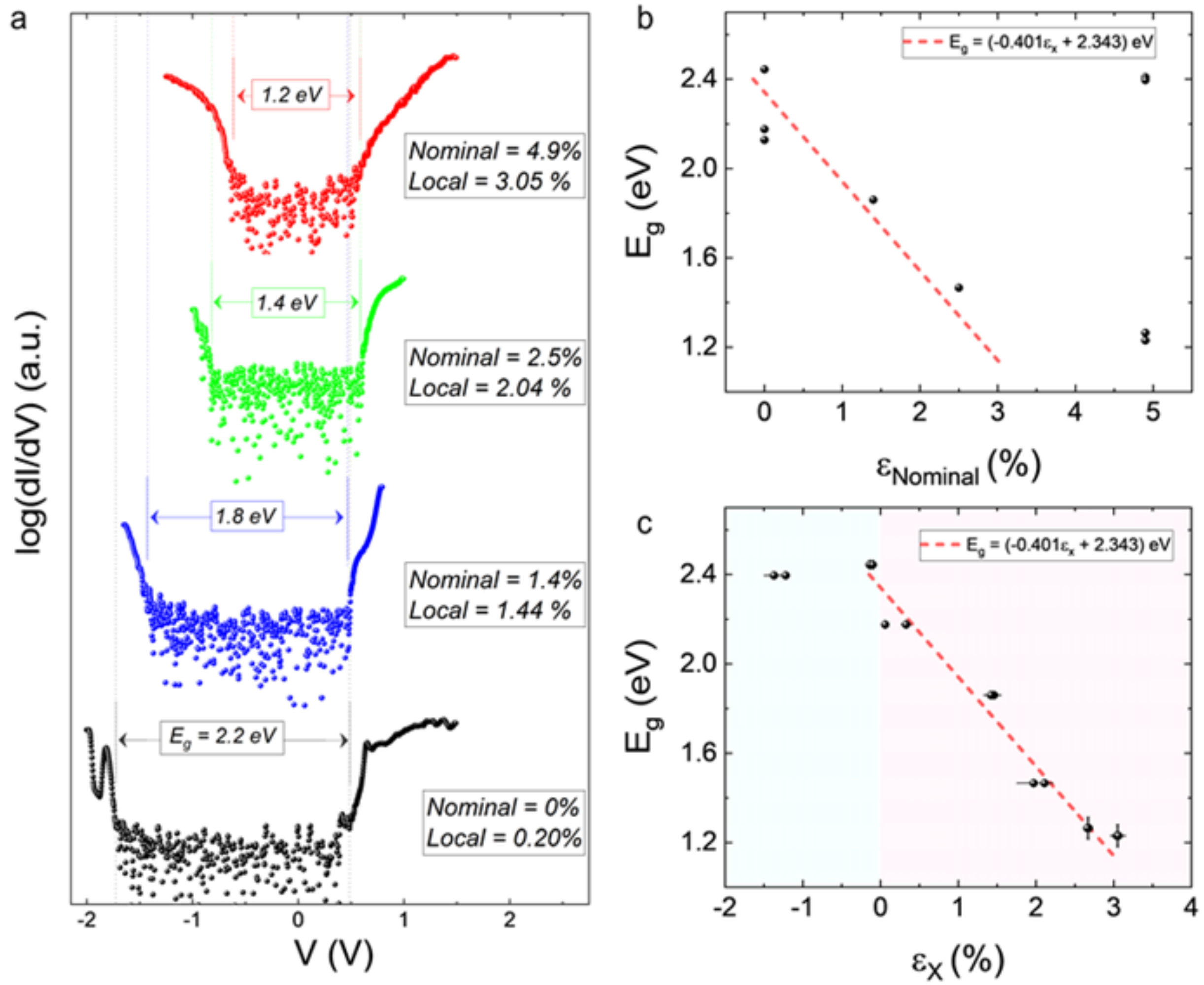

FIG.3

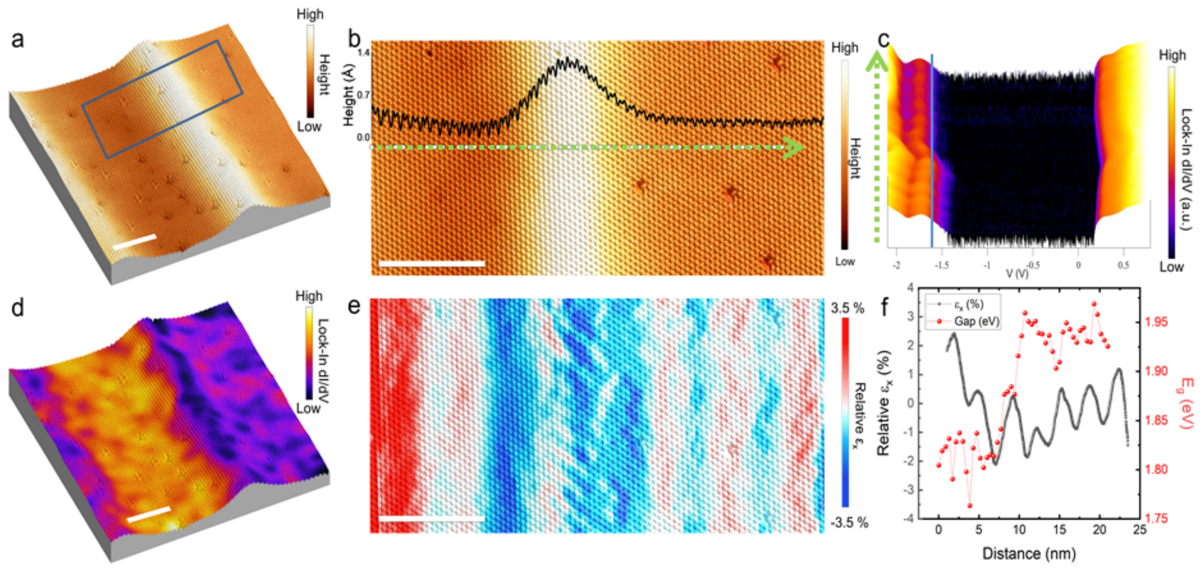

FIG.4

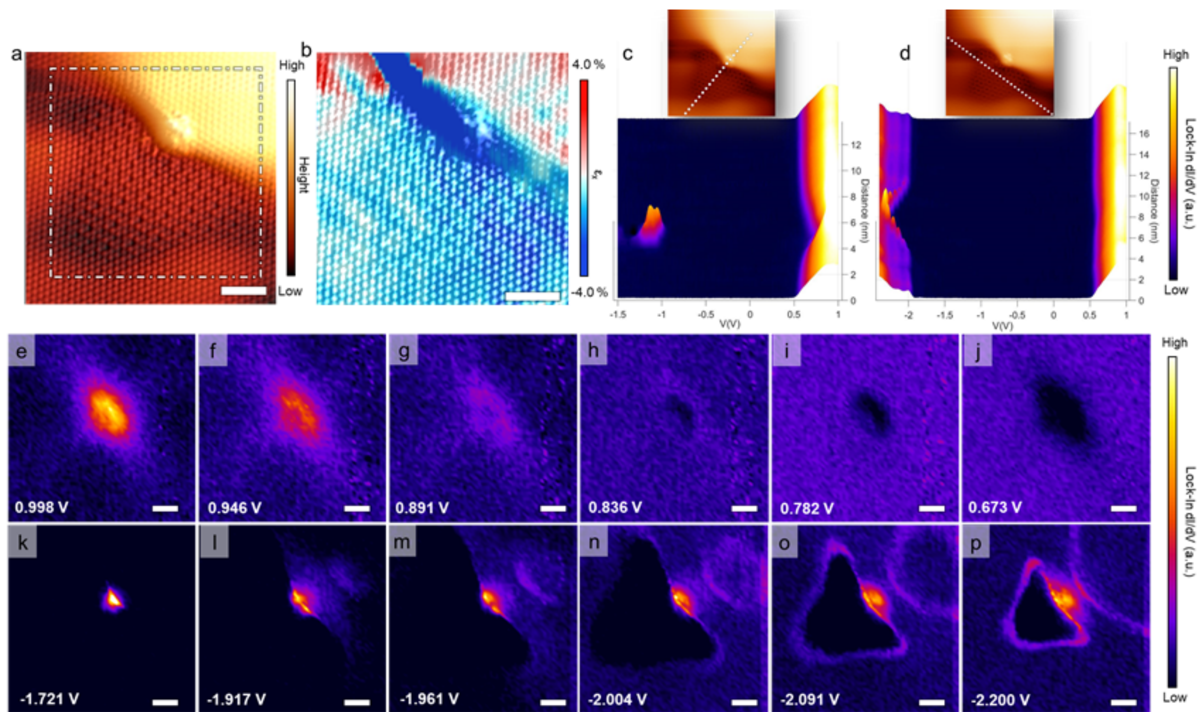

FIG.5

Table of Contents Image